SANDIA REPORT
SAND2019-15043
Printed December 2019

Sandia National Laboratories

Sodium Fire Collaborative Study Progress –CNWG Fiscal Year 2019

David L.Y. Louie (Sandia National Laboratories)
Akihiro Uchibori (Japan Atomic Energy Agency)

Prepared by
Sandia National Laboratories
Albuquerque, New Mexico
87185 and Livermore,
California 94550

Issued by Sandia National Laboratories, operated for the United States Department of Energy by National Technology & Engineering Solutions of Sandia, LLC.

Available to DOE and DOE contractors from
U.S. Department of Energy
Office of Scientific and Technical Information
P.O. Box 62
Oak Ridge, TN 37831

Telephone: (865) 576-8401
Facsimile: (865) 576-5728
E-Mail: reports@osti.gov
Online ordering: http://www.osti.gov/scitech

Available to the public from
U.S. Department of Commerce
National Technical Information Service
5301 Shawnee Rd
Alexandria, VA 22312

Telephone: (800) 553-6847
Facsimile: (703) 605-6900
E-Mail: orders@ntis.gov
Online order: https://classic.ntis.gov/help/order-methods/

ABSTRACT

This report discusses the progress on the collaboration between Sandia National Laboratories (Sandia) and Japan Atomic Energy Agency (JAEA) on the sodium fire research in fiscal year 2019. First, the current sodium pool fire model in MELCOR, which is adapted from CONTAIN-LMR code, is discussed. The associated sodium fire input requirements are also presented. A proposed model improvement developed at Sandia is discussed. Finally, the validation study of the sodium pool fire model in MELCOR carried out by a JAEA's staff is described. To validate this model, a JAEA sodium pool fire experiment (F7-1 test) is used. A preliminary calculation is performed using a modified MELCOR model from a previous experiment simulation. The results of the calculation are discussed as well as suggestions for improvement. Finally, recommendations are made for new MELCOR simulations for next fiscal year, 2020.

ACKNOWLEDGEMENTS

This work is supported by DOE Work Package: AT-19SN02030402. The authors would like to thank Sandia's staff to assist this report, including Andrew Clark who provided the initial MELCOR input deck for the F7-1 test, Larry Humphries, David Luxat and Patrick Mattie for providing suggestions and improvements for this research, K.C. Wagner for providing peer review, and Laura Sowko for editing this report. The authors also like to extend thanks to Takashi Takata of JAEA for providing suggestions and improvements for this research.

CONTENTS

LIST OF FIGURES

LIST OF TABLES

This page left blank

ACRONYMS AND DEFINITIONS

Abbreviation	Definition
CNWG	Civilian Nuclear Energy Research and Development Working Group
CVH	Control volume hydrodynamics package
CVHNAME	Control volume name
DAB	Oxygen diffusion coefficient model switch
FHEAT	Fraction of sensible heat from reactions added to pool
FNA2O	Fraction of Na_2O remaining in pool
FNA2O2	Fraction of Na_2O_2 remaining in pool
FO2	Fraction of oxygen consumed that reacts to form monoxide
Gr	Grashof number
JAEA	Japan Atomic Energy Agency
NAC	Sodium chemistry package
NC	Table row index
NAC_PFIRE	Sodium pool fire mode;
NUM	Number of control volumes
RN	Radionuclide package
Sandia	Sandia National Laboratories
Sc	Schmidt number
Sh	Sherwood number
TOFF	Model deactivation time

Section 2.1 Symbols

Abbreviation	Definition
A_S	Surface area of sodium pool
β	Coefficient of gas expansion
D_{diff}	Gas diffusion coefficient
$\Delta h_{n,Tref}$	Specific enthalpy for compound n evaluated at T_{ref}
$\Delta h_{n,Tm}$	Specific enthalpy of compound n evaluated at the temperature of deposited location either atmosphere (atm) or pool (pool)
f_{O2}	Fraction of the total consumed oxygen that forms Na_2O
f_{x2p}	Deposition fraction of x either Na_2O or Na_2O_2 to the pool
g	gravity
H_G	Gas transport coefficient

Abbreviation	Definition
h_{Na_2O}	Heat of formation for Na_2O
$h_{Na_2O_2}$	Heat of formation for Na_2O_2
$\dot{m}_{O2}$	Oxygen mass consumption rate for pool fire
$\dot{m}_{Na}$	Sodium pool mass burn rate
MW_n	Molecular weight of compound n
q_{bal}	Energy balance
ρ_g	Gas density
P_g	Gas pressure
S	Stochiometric combustion ratio of sodium to oxygen
S_C	Schmidt number
T_g	Gas temperature
T_{ref}	Reference temperature of 298.15 K
T_{surf}	Sodium pool surface
ν	Kinematic viscosity
Y_{O2}	Mass fraction of oxygen

Section 2.2 Symbols

Abbreviation	Definition
Δ_l	Oxide layer thickness
Δt	Timestep
D	Diffusivity of oxygen
D_{eff}	Effective diffusivity of oxygen
δ_i	Thickness of phase i
δ_i^0	Initial thickness which applied to sodium pool layer
F_e	Defined in Equation (2-31)
F_{st}	Fraction of sodium
i	Subscript for phases, sodium or gas, or sodium compound
g	Gravity, subscript for gas
H	Height of liquid
L	Pool diameter

Abbreviation	Definition
λ	Thermal conductivity
λ_{eff}	Effective thermal conductivity
MW_i	Molecular weight of phase i
$\dot{m}_i''$	Mass depletion or production rate per unit area of phase i
μ	Viscosity
ω_i	Molar production rate per volume of phase i
R	Liquid radius
ρ	Density
ϕ	Volume fraction
$\phi_{Na,lim}$	0.95
ε_g	Porosity
r	Subscript r for pool surface
s	Subscript s for solid
T_f	Oxide crust surface temperature
T_∞	Ambient temperature
t	time
u	Characteristic velocity of liquid spreading
V	Volume of liquid
v_i	Velocity of phase i
x	distance
Y	Mass fraction
Y_{O_2}	Oxygen fraction
$Y_{O2,\infty}$	Ambient mass fraction of oxygen

1. INTRODUCTION

This report documents the progress on sodium fire research by Sandia National Laboratories (Sandia) and the Japan Atomic Energy Agency (JAEA) as a part of the Civilian Nuclear Energy Research and Development Working Group (CNWG) between the United States and Japan. In this fiscal year, 2019, we were focusing on the validation of the sodium pool fire model in MELCOR [Sandia 2018a, 2018b]. The sodium pool fire is a complicated phenomenon that occurs from the reaction between oxygen in the air and sodium liquid/vapor on the pool surface [Olivier 2010]. The diffusion of oxygen to the reacting sodium can be limited by the buildup of the oxide layers on the pool surface. The current sodium pool fire model in MELCOR is a parametric model, which may not model these phenomena well.

To assess the current sodium pool fire model in MELCOR, a validation study was performed using a sodium pool fire experiment of the JAEA F7-1 test. First, the current sodium pool fire model in MELCOR is described. Second, a model improvement for the MELCOR pool fire model is presented based on sodium fire study done at Sandia [Olivier 2010]. Then, the comparison results of the MELCOR sodium fire model to the F7-1 experiment is shown. Based on the assessment of the F7-1 experiment, some recommendations are made for model improvement. Finally, the summary and conclusions are presented.

2. SODIUM POOL FIRE MODEL

The sodium pool fire model in MELCOR is adapted from CONTAIN-LMR, which is based on the SOFIRE II code [Sandia 2018a]. The SOFIRE II model was developed from the results of pool fire experiments. The tests concluded that the sodium burning rate was proportional to the oxygen concentration and was controlled by diffusion of oxygen to the pool surface through the convective boundary layer. As observed in the sodium pool fire experiments conducted at Sandia [Olivier 2010], the fire in the sodium pool may depend on the oxide layers and other solidified materials at the surface of the pool. The inclusion of this rate limiting oxide layer is a recommended improvement for sodium pool fire model.

2.1. Current Model

The sodium pool fire model in MELCOR is adapted from CONTAIN-LMR. This model and the input description are described in this section.

2.1.1. Theory

The oxygen mass consumption rate for a pool fire is expressed as a rate equation at the pool surface,

$$\dot{m}_{O2} = A_S H \ \rho_g Y_{O2} \qquad 2\text{-}1$$

where $\dot{m}_{O2}$ is the oxygen mass consumption rate, A_S is the surface area of the sodium pool, H_G is a gas transport coefficient, ϱ_g is the gas density, and Y_{O2} is the ambient mass fraction of oxygen in the atmosphere. The gas transport coefficient is defined as,

$$H \ = 0.14 D_{diff} \left(g \, S_c \frac{\beta}{\nu^2} \left| T_{surf} - T_g \right| \right)^{\frac{1}{3}} \qquad 2\text{-}2$$

where D_{diff} is the gas diffusion coefficient, g is the gravitational constant, S_C is the Schmidt number, β is the coefficient of gas expansion, ν is the kinematic viscosity, T_{surf} is the sodium pool surface temperature, and T_g is the gas temperature. The diffusion coefficient is,

$$D_{diff} = \frac{6.4312 \times 10^{-5}}{P_g} \left[\frac{\left(T_{surf} + T_g \right)}{2} \right]^{1.823} \qquad 2\text{-}3$$

where P_g is the gas pressure. The Schmidt number is:

$$S_c = \frac{\nu}{D_{diff}} \qquad 2\text{-}4$$

The coefficient of gas expansion is,

$$\beta = \frac{1}{0.5 \cdot \left(T_{surf} + T_g \right)} \qquad 2\text{-}5$$

The mass burn rate for sodium is related to the consumption rate of oxygen as,

$$\dot{m}_{Na} = \dot{m}_{O2} S \qquad 2\text{-}6$$

where $\dot{m}_{Na}$ is the sodium pool burn rate and S is the stochiometric combustion ratio of sodium to oxygen. S is defined as follows,

$$S = 2.88 f_{O2} + 1.44(1 - f_{O2}) \qquad 2\text{-}7$$

where f_{O2} is the fraction of the total consumed oxygen that forms Na_2O. An upper limit is imposed on $\dot{m}_{Na}$ such that the amount of sodium burned may not exceed one half of the pool mass within a single timestep.

Unlike the spray fire model, the heat of formations for Na_2O and Na_2O_2, h_{Na_2O} and $h_{Na_2O_2}$, are constants as 9.08e6 and 1.048e7 J/kg, respectively. Based on the user specified value for f_{O2}, the specific heat of combustion at a given reference temperature, T_{ref}, of 298.15 K is computed as:

$$\begin{aligned} q_{com} = & \left(2 f_{O2} MW_{2Na} h_{Na_2O} + (1 - f_{O2}) MW_{2Na} h_{Na_2O_2}\right) \frac{\dot{m}_{O2}}{MW_{O2}} \\ & - \dot{m}_{O2} \Delta h_{O2,Tref} - \dot{m}_{Na} \Delta h_{Na,Tref} \\ & + \left(2 f_{O2} MW_{Na2O} \Delta h_{Na_2O,Tref}\right. \\ & \left. + (1 - f_{O2}) MW_{Na2O2} \Delta h_{Na_2O_2,Tref}\right) \frac{\dot{m}_{O2}}{MW_{O2}} \end{aligned} \qquad 2\text{-}8$$

where, $\Delta h_{n,Tref}$ is the specific enthalpy evaluated at T_{ref} and MW_n is the molecular weight of compound n. The resulting energy balance is given as:

$$\begin{aligned} q_{bal} = & \dot{m}_{O2} \Delta h_{O2,Tatm} + \dot{m}_{Na} \Delta h_{Na,Tatm} + q_{com} \\ & - f_{O2} \dot{m}_{O2} \left(f_{Na_2O,2p} \Delta h_{Na_2O,Tpool}\right. \\ & \left. + \left(1 - f_{Na_2O,2p}\right) \Delta h_{Na_2O,Tatm}\right) \\ & - (1 - f_{O2}) \dot{m}_{O2} \left(f_{Na_2O_2,2p} \Delta h_{Na_2O_2,Tpool} \left(1 - f_{Na_2O_2,2p}\right) \Delta h_{Na_2O_2,Tatm}\right) \end{aligned} \qquad 2\text{-}9$$

Where, $\Delta h_{n,Tm}$ is the specific enthalpy of compound n evaluated at the temperature of the deposition location, either the atmosphere or the pool, and f_{x2p} is the deposition fraction of x, either Na_2O and Na_2O_2, to the pool.

The associated enthalpies are placed into the corresponding field, atmosphere, or pool. The byproduct mass fractions are similarly deposited to the host field for the aerosolized Na_2O and Na_2O_2. Transportation and deposition is treated by MELCOR's Control Volume Hydrodynamics (CVH) and RadioNuclide (RN) packages, respectively.

To provide flexibility of the pool fire model, many of the input parameters described in the equations above can be implemented as control functions, which allows flexibility to explore alternate modeling approaches [Sandia 2018b].

In addition, the sodium spreading on a surface can also be modeled as a function of time or other parameters. This implementation is done through the CV_PDIA record in the CVH package. The CV_PDIA record can linked to a control function that specifies the spreading rate of the sodium. The input format for the sodium pool fire model in the NAC users guide [Sandia 2018b] is described next in Section 2.1.2.

2.1.2. Input Description

Below is the MELCOR input description for this sodium pool fire model.

NAC_PFIRE–Sodium Pool Fire Model
Optional

This record specifies the control volumes where sodium pool fire modeling is permitted. User specified fractions presently give the combustion products as well as the product and energy depositions.

(1) NUM
The number of control volumes permitted for sodium spray pool fire modeling.
(type = integer, default = none, units = dimensionless)

The following data are input as a table with length NUM:

(1) NC
Table row index.
(type = integer, default = none, units = none)

(2) CVHNAME
The name of the control volume.
(type = character, default = none, units = none)

(3) FO2
Fraction of the oxygen consumed that reacts to form monoxide. 1-FO2 is the remaining oxygen fraction for the reaction to form peroxide. A real-value control function may be identified to provide the fraction.
(type = real/character, default = 0.5, units = none)

(4) FHEAT
Fraction of the sensible heat from the reactions to be added to the pool. The balance will go to the atmosphere. A real-value control function may be identified to provide the fraction.
(type = real/character, default = 1.0, units = none)

(5) FNA2O
Fraction of the Na2O remaining in the pool. The balance will be applied to the atmosphere as aerosols. A real-value control function may be identified to provide the fraction.
(type = real/character, default = 1.0, units = none)

(6) FNA2O2

Fraction of the Na_2O_2 remaining in the pool. The balance will be applied to the atmosphere as aerosols. A real-value control function may be identified to provide the fraction.
(type = real/character, default = 0.0, units = none)

(7) TOFF

Model deactivation time. This is useful for modeling experiments.
(type = real, default = 1.0E12, units = seconds)

(8) DAB

Oxygen diffusion coefficient model switch. The default diffusion correlation will be used if a real-value of greater than or equal to 0.0 is specified. A user specified diffusion coefficient can be specified by identifying a real-valued control function.
(type = real/character, default = 0.0, units = m^2/s)

The pool fire model input allows the fraction of oxygen consumed to form sodium monoxide to be modeled as a control function. The corresponding fraction of the sensible heat from the reactions to the pool can be modeled as a control function. The fractions of the sodium monoxide and peroxide remaining in the pool also can be modeled as a control function. These fractions are important because the available oxygen and sodium in the air and in the pool, respectively, have significant influences in the formation of the oxide layers and disappearance of the layer(s). Finally, the oxygen diffusion coefficient in Equation 1-3 can be modeled as a control function that represents changes in the rate of oxygen diffusion to the sodium and its products oxide layers on the pool surface.

To model spreading of the sodium pool from an experiment, the pool cross sectional area can be modeled using control functions.

2.2. Model Improvement

Based on insights from Sandia sodium experiments [Olivier 2010], some improvements to the existing pool fire model are proposed. Figure 2-1 shows the one-dimensional layers of the sodium pool and their associated temperature profile and oxygen fraction magnitudes. As long as the sodium pool remains in the liquid state (above 371 K at atmospheric conditions), there is an oxide crust with aerosol generation. Because the melting temperatures of sodium peroxide and monoxide are significantly different, 948 K and 1405 K, respectively, the disappearance of the peroxide layer in the pool may be possible, particularly if the pool temperature is above the melting point of the peroxide layer. Other potential improvements include the treatment of liquid sodium spreading. Section 2.2.1 describes a simplified spreading model. Section 2.2.2 describes a new model for the formation of oxide layers in the sodium pool.

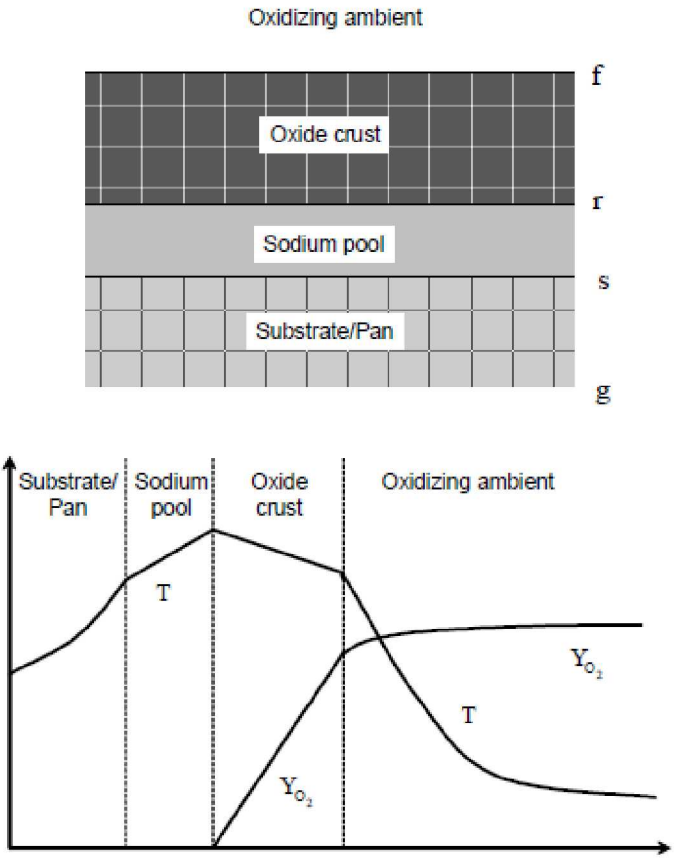

Figure 2-1 Schematic of the pool layers, temperature Profile (T), and Oxygen Fraction (Y_{O2}) [Olivier 2010]

2.2.1. Liquid Sodium Spreading

This model is adapted from the pancake spreading model in the Cavity (CAV) package [Sandia 2018a], where a molten corium spreading is modeled. The pancake spreading considers both viscous and gravitational forces.

The drop height of the sodium flow onto the pool surface is assumed to be very small, so that no heat transfer or reaction is assumed. However, depending on the mass flow of the liquid sodium into the pool, the spreading on the floor (or pan, in experiments) varies. As a simplification, it is assumed that the sodium fire does not influence the viscosity of the liquid mixture. A simplified pancake spreading model (with a radius, R and a height, H) can be assumed that can be driven by the gravitational forces that are opposed by viscous forces in a laminar flow regime. The balance of these two forces can be expressed in terms of pressures by,

$$\mu \frac{u}{H^2 R} \propto \rho g H \qquad 2\text{-}10$$

where μ and ρ are the viscosity and density of the sodium, respectively, and g is the gravity. u is the characteristic velocity of the sodium spreading, which can be given by dR/dt. If the height of the sodium is approximately constant in dt, then replacing the above equation with an equal size then it becomes,

$$\frac{dR}{dt} = C\frac{\rho g}{\mu \pi^3}\frac{V^3}{R^7} \quad \text{2-11}$$

Where C is a constant. Solving the above equation as integral over time, it becomes

$$R(t+\Delta t) = \sqrt[8]{R(t)^8 + C \cdot \frac{\rho\, g}{\mu\, \pi^3} V^3(t)} \quad \text{2-12}$$

If the mass flow rate, $\dot{m}$ for spreading remains constant during a timestep (Δt), then the volume related to mass (m) is given by $\frac{m}{\rho}$. Equation 2-12 can be rewritten as,

$$R(t+\Delta t) = \sqrt[8]{R(t)^8 + C \cdot \frac{g}{\mu\, \pi^3 \rho^2} \dot{m}^3(t)^4} \quad \text{2-13}$$

2.2.2. Oxide Layers

The effect of the oxide layer buildup may influence the sodium fire in the pool [Olivier 2010]. This section describes the oxide layer buildup model from [Olivier 2010].

Because liquid sodium can react with the oxygen when diffused closely together, the two main reactions[1] are,

$$Na + \frac{1}{4}\, O_2 \rightarrow \frac{1}{2} Na_2O \quad \text{2-14}$$

$$Na + \frac{1}{2}\, O_2 \rightarrow \frac{1}{2} Na_2O_2 \quad \text{2-15}$$

As shown above in these two reactions, when there is insufficient oxygen (i.e., below stoichiometric), the first reaction with monoxide is the primary product. The second reaction with the peroxide is the product when there is ample oxygen (i.e., above stoichiometric). However, there is no specified oxygen level that defines the transition between the above two reactions.

Once the sodium oxide products are formed, the subsequent reactions with oxygen and sodium include,

$$Na_2O + \frac{1}{2}\, O_2 \rightarrow Na_2O_2 \quad \text{2-16}$$

$$\frac{1}{2} Na_2O_2 + Na \rightarrow Na_2O \quad \text{2-17}$$

Equations 2-16 dominate when oxygen is available while Equation 2-17 is the occurs when only sodium is present.

[1] Note that only oxygen reactions are considered. The moisture in the air or from water can also react with sodium to form sodium hydroxide and hydrogen.

2.2.2.1. Formation of Oxide Layers

In sodium pool fire experiments, an oxide crust layer is visible on the surface of the pool under certain conditions. The continued heat release with this visible oxide crust suggest that oxygen continues to diffuse through the oxide crust. However, the crust surface porosity and the nature of pores (or open pore structure) require further characterization and understanding.

Furthermore, an uncertainty remains whether sodium oxide remains near the surface of the pool. In comparing the density, Na_2O_2 has a higher value than that of Na_2O. This difference may allow the peroxide to sink below the surface of the pool and the reaction in Equation 2-17 may take place to form the monoxide. Sodium monoxide is a solid (due to its higher melting point) and would be presumably porous. The existence of the solid monoxide matrix would provide a support structure for a peroxide crust at the pool surface.

The mechanics of these solid layers within the pool and at the pool surfaces are not well understood. The continual presence of an oxide crust has been observed in the experiments, but it does not thicken until a non-negligible fraction of the sodium has been oxidized. This fraction may be relatively constant and increase linearly as the pool depth increases. The presence of oxide crust from monoxide solid to the formation of peroxide crust above the pool surface continues as pool depth increases to a point. After this point, the oxide crusts thicken as the sodium pool recedes due to oxidation processes.

The porosity of the oxide layer(s) can be characterized using the Philling-Bedworth ratio, which is the oxide volume to metal volume ratio. For sodium peroxide and monoxide, this ratio is calculated to be 0.58 and 0.57, respectively. So, they are very similar. The porosity may be due to the presence of air and liquid sodium that permeate to the oxide crust as two multiphase regions: one region with air plus oxide and one region with sodium plus oxide (see Equations 2-16 and 2-17 explanations above).

Using the assumption that a multiphase region only consists no more than 2 phases, the gas-phase volume fraction (ϕ_g) is related to that of sodium peroxide ($\phi_{Na_2O_2}$):

$$\phi_g = 1 - \phi_{Na_2O_2} \qquad 2\text{-}18$$

For the sodium plus oxide region, the sodium-phase volume fraction (ϕ_{Na}) is related to that of sodium monoxide (ϕ_{Na_2O}) as,

$$\phi_{Na} = 1 - \phi_{Na_2O} \qquad 2\text{-}19$$

With the phase ϕ volume fractions and densities assumed to be constant in a continuity equation, the velocity (v_i) and the mass depletion or production rate per unit area ($\dot{m}_i''$) for phase i can be related as:

$$v_i = \frac{\dot{m}_i''}{\phi_i \rho_i} \qquad 2\text{-}20$$

The total thickness (δ) of the layers for relevant phases can be obtained from the time integral of this equation,

$$\delta_i - \delta_i^0 = \frac{1}{\phi_i \rho_i} \int_0^t \dot{m}_i'' \, dt \qquad 2\text{-}21$$

δ_i^0 is the initial-layer thickness, which applied to sodium pool layer before other layers can be formed. Assuming a 1-dimension solution, the oxide layer with a porosity would always be lighter than liquid sodium as shown in Figure 2-1. The porous oxide layer above the sodium pool may allow oxygen to diffuse to the sodium.

Two distinct phases of the oxide layer are expected. In the first phase, the oxide layer is sinking, which is described in Section 2.2.2.2. In the second phase, the oxide forms a crust at the pool surface, which is described in Section 2.2.2.3.

2.2.2.2. Oxide-Sinking Phase

An oxide layer can exist in two forms: Na_2O in the presence of excess Na and Na_2O_2 in the presence of O_2. Aerosols of Na_2O_2 exist in the ambient oxidizing flow when there is sufficient oxygen. The oxide tends to stick to Na_2O if it comes into contact with Na. Na_2O may sink into the pool unless the deposited Na_2O has reached a suitable buoyancy that provides support for the growth of an oxide layer at the pool surface. The mass flux for Na_2O that sticks to the pool surface is a function of the fraction of sodium (F_{st}) [Olivier 2010].

$$\dot{m}''_{Na2O} = -\frac{F_{st}}{2} \frac{MW_{Na2O}}{MW_{Na}} \dot{m}''_{Na} \qquad 2\text{-}22$$

On the other hand, the amount of aerosol as Na_2O_2 is given by:

$$\dot{m}''_{Na2O2\,(aerosol)} = -\frac{(1 - F_{st})}{2} \frac{MW_{Na2O2}}{MW_{Na}} \dot{m}''_{Na} \qquad 2\text{-}23$$

The amount of sodium consumed for this reaction is given by the oxygen mass in contact with sodium, for which the amount of Na consumed is given by,

$$\dot{m}''_{Na} = \left(\frac{4}{2 - F_{st}}\right) \frac{MW_{Na}}{MW_{O2}} \dot{m}''_{O2} \qquad 2\text{-}24$$

Then both Equations 2-22. and 2-23. can be re-written as functions of oxygen mass flow,

$$\dot{m}''_{Ns2O} = -\left(\frac{2F_{st}}{2 - F_{st}}\right) \frac{MW_{Na2O}}{MW_{O2}} \dot{m}''_{O2} \qquad 2\text{-}25$$

$$\dot{m}''_{Na2O2\,(aerosol)} = -2\left(\frac{1 - F_{st}}{2 - F_{st}}\right) \frac{MW_{Na2O2}}{MW_{O2}} \dot{m}''_{O2} \qquad 2\text{-}26$$

In terms of the phase volume fraction and thickness, the following equations are considered,

$$\frac{d\delta_{Na}}{dt} = \frac{\dot{m}''_{Na}}{\rho_{Na}} + \frac{\dot{m}''_{Ns2O}}{\rho_{Na2O}} \quad 2\text{-}27$$

The thicknesses of sodium and oxide layers are assumed to be same until the ϕ_{Na} reduces to $\phi_{Na,lim}$ which is 0.95.

$$\frac{d\phi_{Na}}{dt} = \frac{1}{\delta_{Na}}\left[(1-\phi_{Na})\frac{\dot{m}''_{Na}}{\rho_{Na}} + \phi_{Na}\frac{\dot{m}''_{Ns2O}}{\rho_{Na2O}}\right] \quad 2\text{-}28$$

The oxide crust can continue to grow at this fraction. Any additional deposited oxides remain at the pool surface as long as the temperature is below 600°C, a transitional temperature.

2.2.2.3. Oxide-Crust Phase

Based on the models developed in Section 2.2.2.2 for the oxide-sinking phase, the oxidation of sodium and monoxide leads to the production of peroxide when $\phi_{Na} = \phi_{Na,lim}$. The mass flux of Na, Na2O, and Na2O2 can be calculated as [Olivier 2010]:

$$\dot{m}''_{Na} = \left(\frac{2}{1+F_e}\right)\frac{MW_{Na}}{MW_{O2}}\dot{m}''_{O2} \quad 2\text{-}29$$

$$\dot{m}''_{Na2O} = \left(\frac{2F_e}{1+F_e}\right)\frac{MW_{Na2O}}{MW_{O2}}\dot{m}''_{O2} \quad 2\text{-}30$$

$$\dot{m}''_{Na2O2} = \left(\frac{1+2F_e}{1+F_e}\right)\frac{MW_{Na2O2}}{MW_{O2}}\dot{m}''_{O2} \quad 2\text{-}31$$

$$\text{where } F_e = \frac{MW_{Na}}{MW_{Na2O}}\frac{\rho_{Na2O}}{\rho_{Na}}\left(\frac{1-\phi_{Na}}{\phi_{Na}}\right)$$

2.2.2.4. Oxide Crust Characteristics

The porosity of the oxide crust will have a significant effect on the heat and mass transfer through the crust layer. When a crust is present, the heat flow by thermal conduction and mass transfer through diffusion of oxygen is required. The effective thermal conductivity (diffusivity), λ_{eff}, which includes the oxide solid (Na_2O) and air plus porosity are related as follows,

$$\frac{\lambda_{eff}}{\lambda_g} \approx \frac{2\varepsilon_g}{\varepsilon_g} \quad 2\text{-}32$$

In this equation, ε_g is the porosity (1-ϕ_s).

For diffusion, the effective mass diffusion of oxygen (D_{eff}) in this porous media is given by Maxwell's equation:

$$\frac{\varepsilon_g D_{eff}}{D} = \frac{2\varepsilon_g}{3-\varepsilon_g} \qquad 2\text{-}33$$

where D is the appropriate gas-phase diffusivity (oxygen in nitrogen). Generally, $D_{eff} = D{\varepsilon_g}^{m-1}$, which the exponent, m is the Bruggemann exponent and typically a value of 1.5 is used which agrees well with Eq. (2-33). However, a larger exponent was recommended in the literature [Olivier 2010]. Figure 2-2 shows the plot of the ratio of $(D_{eff}/D)/(\lambda_{eff}/\lambda)$ through a porous oxide layer as a function of porosity (phase volume fraction).

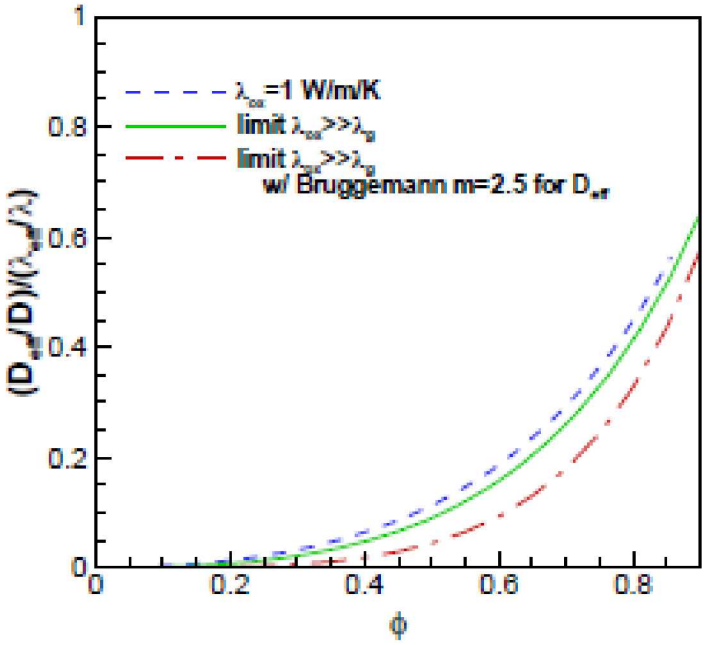

Figure 2-2. The ratio of to the effective mass diffusivity, D to thermal diffusivity, λ through a porous oxide crust as function of porosity, ϕ [Olivier 2010].

2.2.2.5. Oxygen Mass Rate

In air, oxygen or sodium vapors exist with nitrogen in the porous-media species conservation equation,

$$\frac{\partial(\varepsilon_g \rho_g Y_i)}{\delta t} + \frac{\partial(\varepsilon_g \rho_g u_g Y_i)}{\delta x} = \frac{\partial}{\partial x}\left(\varepsilon_g \rho_g D_{eff} \frac{\partial Y_i}{\partial x}\right) + MW_i \omega_i \qquad 2\text{-}34$$

Where Y is the species mass fraction within a phase, and that species has D_{eff} which is simply a binary diffusion coefficient between oxygen and nitrogen, D. u_g is the phase velocity, and MW is the molecular weight of the phase, i. ω is the molar production rate (per volume of phase i).

There are two conditions for which oxidation can occur at the pool surface. The first one is at low temperature where the oxide crust is present, and the sodium vapor pressure is negligible (sodium

vapor pressure at 600ºC is 0.02 atmosphere). Thus, no reaction occurs at the gas phase. There is only the reaction on the liquid sodium's surface. When the pool temperature reaches higher temperatures, the vapor pressure increases, which increases the amount of sodium vapor. Consequently, a gas phase reaction can occur at high temperatures as the sodium vapor concentration increases. Sections 2.2.2.5.1 and 2.2.2.5.2 describe the computation of mass flux of oxygen for the low and high temperature conditions, respectively.

2.2.2.5.1. Low-Temperature Oxidation

The mass flux of oxygen for low-temperature oxidation can be described using the Sherwood number (Sh), its characteristic length, and the pool diameter [Olivier 2010].

$$\dot{m}''_{O2} = \left(\frac{Sh}{L}\right)\frac{\rho_g D\, Y_{O2,\infty}}{1+\delta/\Delta_l} \qquad 2\text{-}35$$

Where the oxide layer thickness is normalized by the characteristic length scale,

$$\Delta_l = \left(\frac{D_{eff}}{D}\right)/\left(\frac{Sh}{L}\right) \qquad 2\text{-}36$$

Sh in Equations 2-35 and 2-36 are given for flow conditions in a circular pool.

In the turbulent flow regime,

$$Sh = 0.16(rSc\ )^{1/3} \qquad 2\text{-}37$$

In the laminar flow regime,

$$Sh = 0.7(rSc\ )^{1/4} \qquad 2\text{-}38$$

Where Gr is the Grashof number and Sc is the Schmidt number in the above equations is given as:

$$r\ = \left(\frac{T_f - T_\infty}{T_\infty}\right)\left(\frac{g}{\mu_a^2}\right)L^3 \qquad 2\text{-}39$$

T_f =oxide crust surface temperature, T_∞=ambient temperature, L=pool diameter, μ_a=air viscosity, and g=gravity. In the turbulent regime, the ratio of Sh/L will be independent of the pool diameter.

2.2.2.5.2. High-Temperature Oxidation

At the higher temperatures, the sodium vapor pressure is non-negligible. Thus, the oxidation can occur at the gas phase. The oxygen mass flux is given as [Olivier 2010]:

$$\dot{m}''_{O2} = \left(\frac{Sh}{L}\right)\left(\frac{\rho_g D}{1+\delta/\Delta_l}\right)\left(Y_{O2,\infty} + \frac{1}{2}\frac{MW_{O2}}{MW_{Na}}Y_{Na,r}\right) \qquad 2\text{-}40$$

Where subscript r is at the pool surface.

3. MELCOR VALIDATION STUDY

This section describes the validation of the pool fire model in MELCOR using the JAEA F7-1 sodium pool fire experiment [Futagami 1998]. In a separate effort, JAEA is performing a validation of the JAEA SPHINCS code using Sandia's P1 and P3 outdoor pool fire experiments. Section 3.1desribes the JAEA F7-1 experiment. Section 3.2 describes the MELCOR input model of the F7-1 experiment. The MELCOR model described in Section 3.2 was adapted from a previous input model [Clark 2019]. Section 3.3 describes the comparison of MELCOR using the F7-1 data. Finally, Section 3.4 provides recommendations for future validation work.

3.1. F7-1 Test Description

The test apparatus, shown in Figure 3-1, consists of the stainless-steel vessel, the liquid sodium discharging system, the stainless-steel catch pan, the thermal insulator, the air ventilation (purge) line, and the measurement system. The test vessel is about 2.2 m in height and 1.3 m in diameter. The nozzle exit is located at 0.1 m height from the catch pan. The thickness of the catch pan is 6 mm. The catch pan was attached to two 50 mm layers of thermal insulation. The liquid sodium was discharged with the average leak rate of 3.28 g/s for 1,505 seconds. The liquid sodium fell with a column shape and formed a pool on the catch pan. The final area of the sodium pool was 0.28 m^2. The air in the vessel was ventilated with a steady flow of approximately 3.0 m^3/min. The test conditions are summarized in Table 3-1.

The experimental temperature measurements of the vessel surface, the atmosphere, the pool, the bottom surface of the catch pan, and the surface between the two-thermal insulation layers were monitored with multiple thermocouples. The concentrations of the oxygen, the hydrogen, and the aerosol were also measured in this test. The measured values used for comparison with the computational results were obtained from [Futagami 1998].

Table 3-1. Test conditions

Parameter	Data
Sodium temperature	505 °C
Sodium leak form	Column
Sodium leak height	0.1 m from catch pan
Sodium leak duration	1505 s
Average sodium leak rate	3.28 g/s
Total leak quantity of sodium	4.94 kg
Oxygen concentration (initial)	20.8%
Atmosphere temperature (initial)	12.7 °C
Atmosphere relative humidity	49.2%
Ventilation flow rate	Approximately 3.0 m^3/min

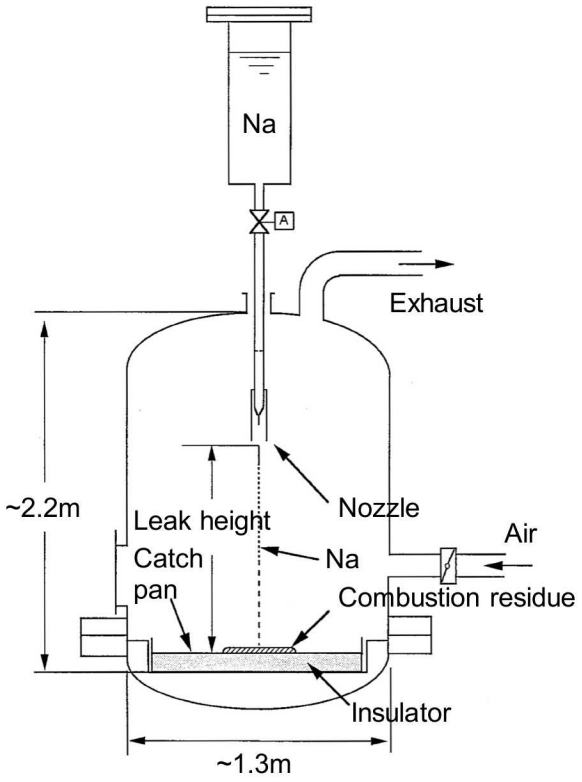

Figure 3-1. Test apparatus

3.2. MELCOR Model

Similar to the previously developed MELCOR model [Clark 2019], the MELCOR model used three control volumes and the two flow paths as shown in Figure 3-2. The current model included some modifications from the previous MELCOR model [Clark 2019]. As shown in Figure 3-2, the control volume "FRAT" corresponds to the vessel of the F7-1 test. The spray and pool fire occur in this control volume. The "PREENV" and "ENV" correspond to the environment as shown in Figure 3-2. The time-independent option is applied for these two control volumes. The velocities at the two flow paths were 5.74 m/s throughout the computation, which corresponded to 3.0 m^3/min in the pipe with the cross-sectional area of 8.71×10^{-3} m^2. There are three heat structures; the rectangular "top head," the cylindrical "wall," and the rectangular "bot head". The top head and wall have thermal properties of stainless steel. The "bot head" is divided into the stainless-steel pan and the thermal insulation layer. Each heat structure is divided into the conduction mesh nodes. Natural convection and radiation heat transfer occur between the surface of each heat structure, the pool, and the atmosphere. The input parameters for heat transfer and sodium fire computation are summarized in Table 3-2 and Table 3-3, respectively. The radiation view factors of the top head and wall are specified according to the ratio of the surface area. The view factor of the bot head is 0.0 because only natural heat transfer takes place between the pool and the bot head. The initial temperature of the atmosphere and all of the heat structures were set to the same value.

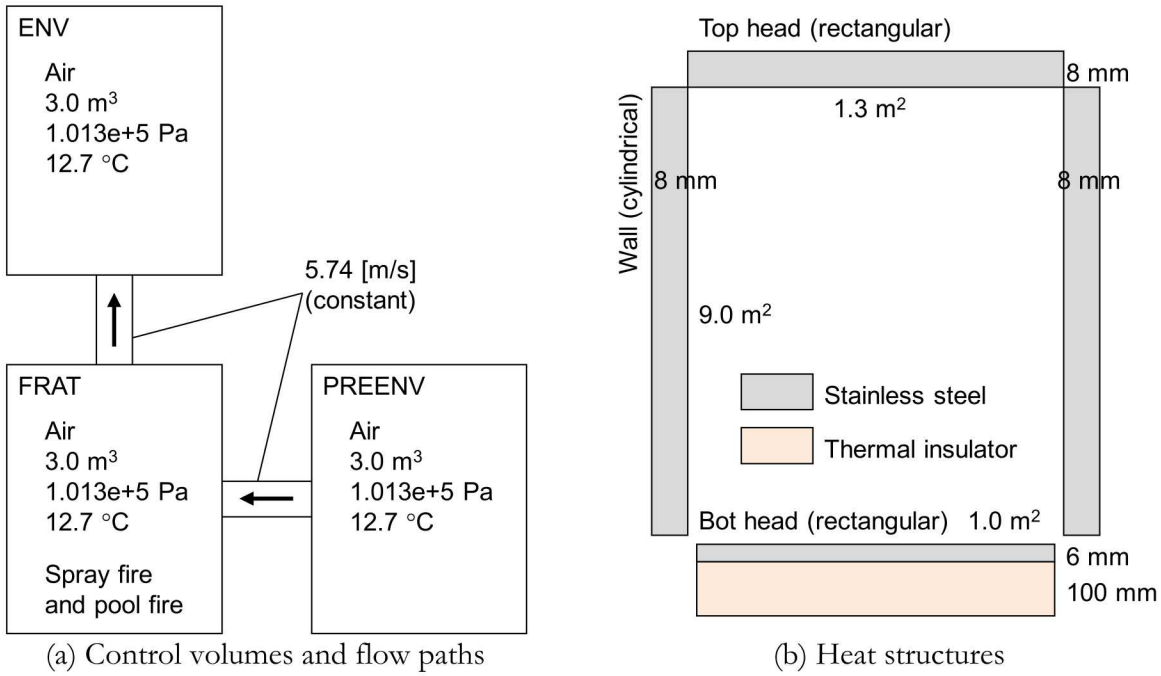

Figure 3-2. MELCOR model setup. Note both ENV and PREENV are modeled as a time independent volume.

Table 3-2. Computational conditions of heat transfer in base case

Natural convection heat transfer coefficient		6.08 W/(m^2-K)
Radiation model		Gray gas model
Emissivity of heat structure surface		0.90
Emissivity of pool surface		0.98
View factor	Top head	0.13
	Wall	0.87
	Bot head	0.00

Table 3-3. Computational conditions of sodium spray and pool fire in base case

Spray fire	Height	0.1 m
	Droplet diameter	0.0045 m
	FNA2O2	1.0
	Time step	Terminal velocity model
Pool fire	FO2	0.6
	FHEAT	0.8
	FNA2O	0.5
	FNA2O2	0.5
	TOFF	2760.0 s
	DAB	0.0 m^2/s

3.3. Simulation Results and Discussions

This section describes the MELCOR simulations using the model described in Section 3.2. MELCOR 2.2 Version 11932 was used to perform these MELCOR simulations. Section 3.3.1 describes the base case simulation. Section 3.3.2 describes the results of sensitivity analysis.

3.3.1. Base Case

Figure 3-3 compares the calculated pool temperature with some of the measured values. The light-blue line corresponds to the end of sodium leak. The two measured values show a temperature increase after contact with the spreading sodium pool. On the other hand, the calculated temperature increased immediately after the start of the computation because the MELCOR code has a single, lumped temperature approximation for the pool. The calculated and measured temperatures remained high during the experiment due to the pool fire. The fire extinguished after 2,730 seconds in the base case, which resulted in a code failure because the pool fire physics model was not turned off. To avoid the MELCOR code failure, the pool fire computation was turned off at 2,730 seconds by enabling the input parameter "TOFF" parameter. The pool mass at 2,730 seconds was 53.6 g. After turning pool fire computation off, the pool temperature dropped rapidly from 640°C to 100°C over approximately 50 seconds. The rapid cooling behavior is attributed to the heat removal by the catch pan.

Figure 3-4 compares the calculated atmosphere temperature and some of the measured values. The various atmosphere thermocouples show a temperature rises from about 50°C to over 150°C before the end of sodium leak in the test. The calculated temperature varied within the distribution range in the test and increased up to the same level with the maximum valued in the test. The temperature dropped after turning pool fire computation off. This is due to the end of the fire and air ventilation removing.

Figure 3-5 and Figure 3-6 compare the calculated vessel head and wall inner surface temperatures with the measured values, respectively. The maximum difference between the calculated and measured vessel head temperature is less than 50°C. The temperature of the heat structures is strongly affected by the radiation view factor. The vessel head view factor was estimated using the ratio of the surface area of each heat structure using the surface to surface exchange model. The net enclosure radiation model was not used in this simulation. The enclosure radiation model performs multiple surface exchange with an intermediate participating media (e.g., the smoke, which is a by-product of the sodium fire). The enclosure radiation model is recommended for future work.

Figure 3-7 compares the calculated catch pan bottom surface temperature and experimental data. The measured temperature shows a substantial increase in response to the burning sodium. In fact, the peak measured pan is the same as the pool temperature. On the other hand, the calculated pan temperature only rose to 100°C. There are the following two possible reasons for this discrepancy. The natural convection heat transfer coefficient between the pool and the catch pan was set to a constant value as shown in Table 3-2. The calculated heat transfer coefficient does not accurately reflect contact with a sodium pool. The one-dimensional heat transfer surface does not vary the surface temperature in the radial direction of the catch pan even though the pool area (0.00 ~ 0.28 m^2) is smaller than the surface area of the catch pan (1.00 m^2). Consequently, the catch pan temperature reflects the average of sodium region and the uncovered region. One possible solution is to use multiple heat structures to represent the pan surface.

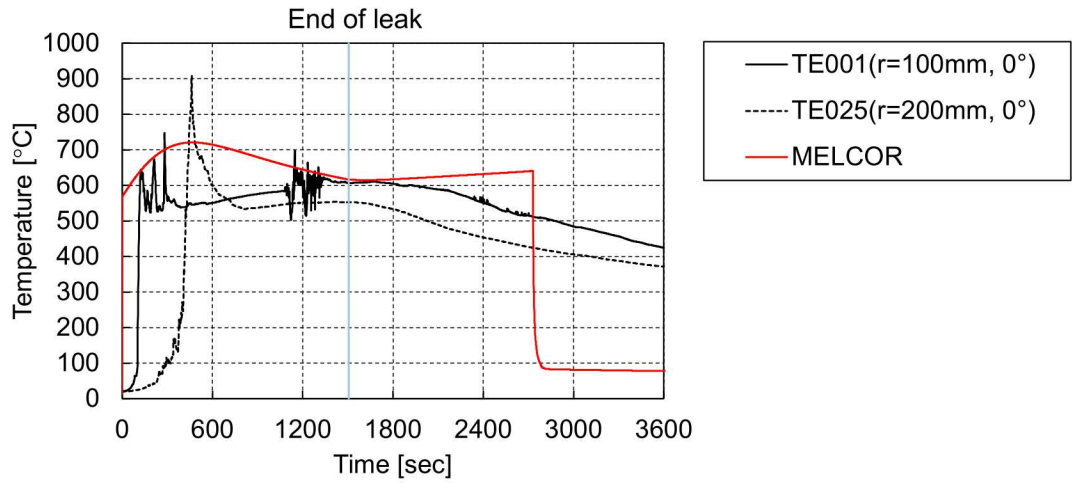

Figure 3-3. Pool temperature comparison

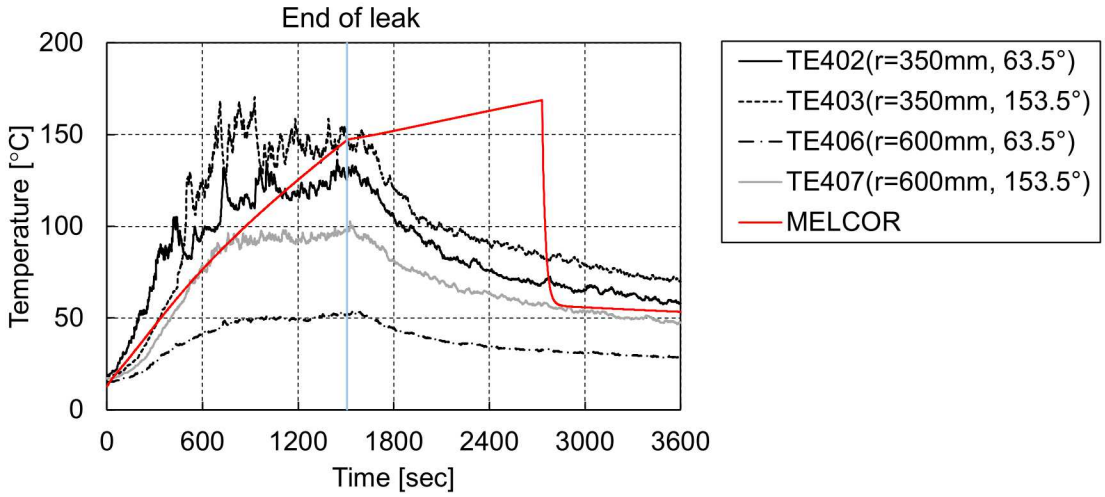

Figure 3-4. Atmosphere temperature comparison

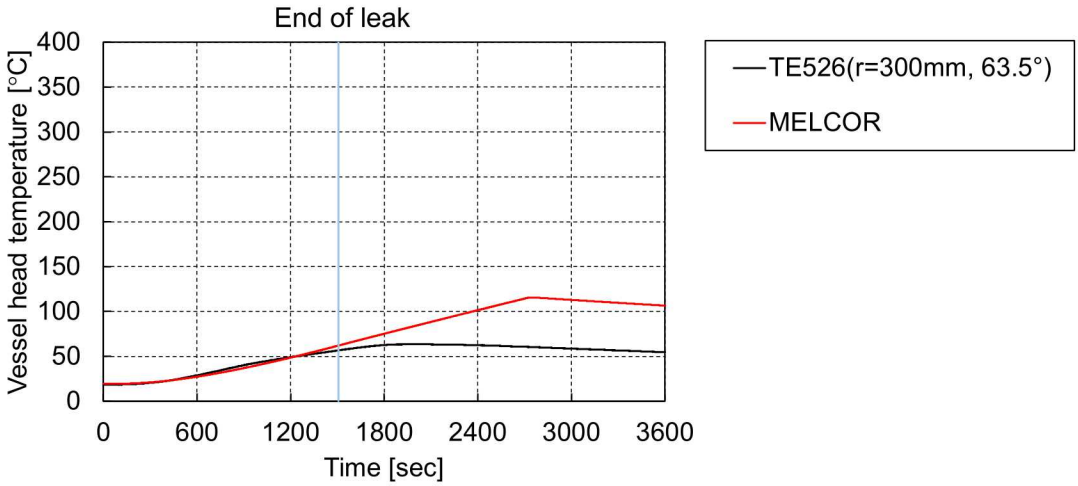

Figure 3-5. Vessel head inner surface temperature comparison

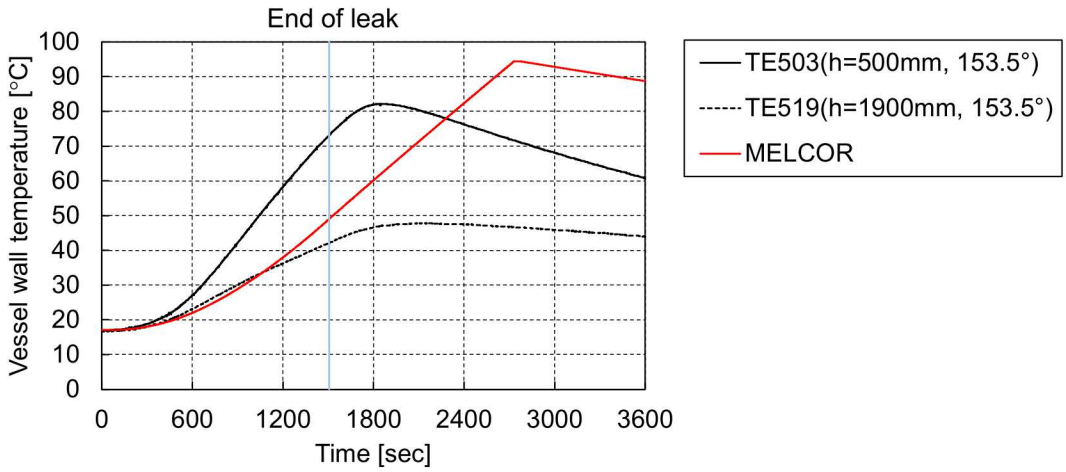

Figure 3-6. Vessel wall inner surface temperature comparison

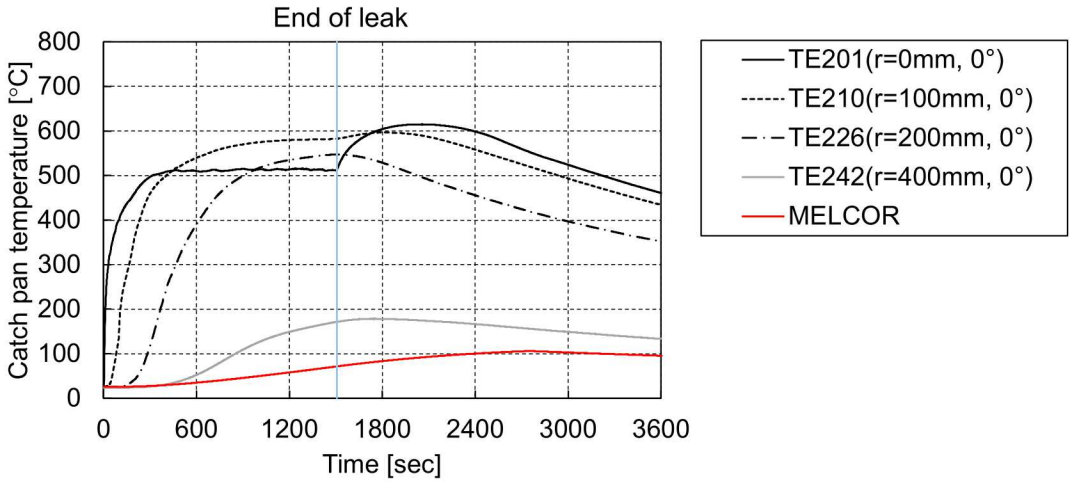

Figure 3-7. Catch pan bottom surface temperature comparison

3.3.2. Sensitivity analysis

Several input parameters (see Section 2.1.2) may influence the temperature transition; therefore, a study was conducted. In this study, only FHEAT and DAB input parameters were varied from the base case described in Section 3.3.1.

The FHEAT input parameter specifies the fraction of reaction heat added to the pool. The excess reaction heat goes to atmosphere. Figure 3-8 shows a comparison of 0.4 and 0.6 for FHEAT. The pool temperature in the case of 0.6 is higher than that of 0.4. The atmosphere temperature in the case of 0.6 is lower than the 0.4 calculation. This result is consistent to the definition of FHEAT. If FHEAT is too large, there is numerical instability due to the extreme values in the sodium properties as the sodium mass is exhausted.

The computational method for pool fire in MELCOR is based on the experimental knowledge that the sodium burning rate is proportional to the oxygen concentration and is controlled by diffusion of oxygen to the pool surface through a convective boundary layer. An oxygen diffusion coefficient given by Equation 1-3 is specified by the input parameter DAB. The default value of DAB is 0. From the conditions at 1,505 seconds (P_g=146675 Pa, T_g=420.00 K, T_{surf}=889.52 K), the DAB

diffusion coefficient is calculated to be 5.97×10^{-5} m^2/s. Figure 3-9 shows the sensitivity of DAB using values of 0 m^2/s (default) , 5.97×10^{-5} m^2/s, and 1.0×10^{-4} m^2/s. The difference between DAB equal to 5.97×10^{-5} m^2/s and the base case (0.0 m^2/s) is relatively small. When DAB is increased to 1.0×10^{-4} m^2/s, both pool and atmosphere temperature are higher because of the increased the sodium burning rate with higher diffusion (i.e., see Equations 1-1 to 1-4). However, DAB depends on the instantaneous pressure and temperature and should be evaluated by using a control function.

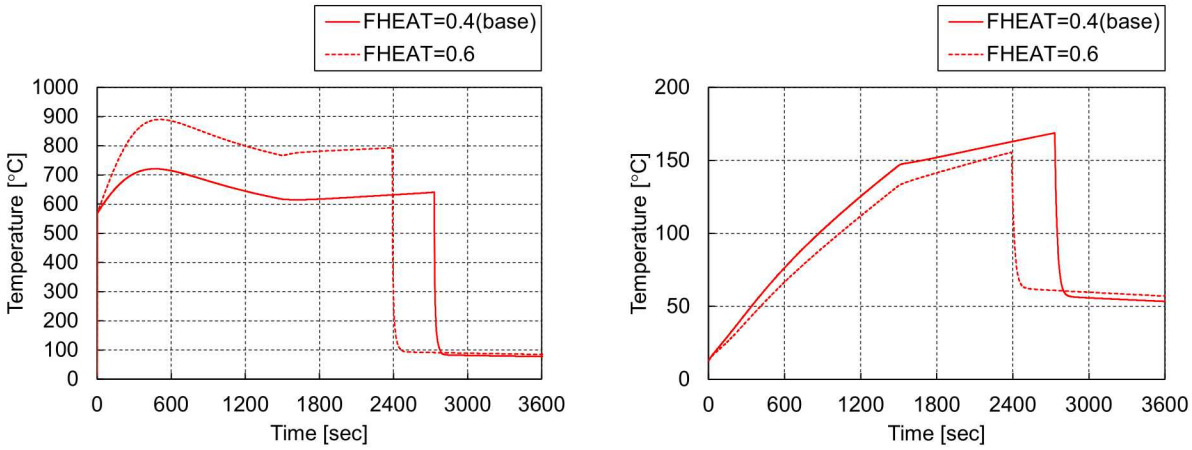

(a) Pool temperature (b) Atmosphere temperature

Figure 3-8. Effect of input parameter FHEAT

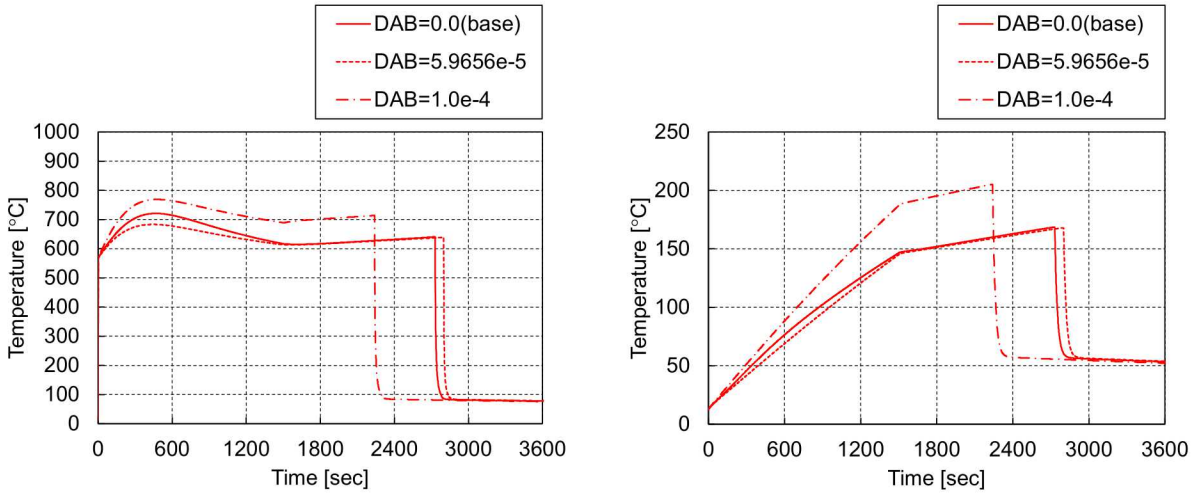

(a) Pool temperature (b) Atmosphere temperature

Figure 3-9. Effect of input parameter DAB

3.4. Recommended Future Studies

The previous two sections describing the progress of the MELCOR validation study in fiscal year 2019. While the results are encouraging, several areas for improvement have been identified. Although not mentioned previously, some numerical instability issues were identified in the sodium properties that needed to be resolved.

The following recommendations are made for future studies. Some improvements are needed to the MELCOR input model that represents the F7-1 test. The purge line flow to the test vessel ("FRAT" control volume) during the sodium fire may affect the thermal hydraulic behavior observed in MELCOR as compared to the test data. It is recommended to examine the sensitivity of the purge line modeling. Note that the current MELCOR model imposes constant velocity flows from the "PREENV" and "ENV" control volumes, which may be different from the experiment where only the outflow (purge line) was used. This may include varying the flow rate of the purge line.

Another observation identified in this validation study is that the single heat structure in MECLOR representing the catch pan ("bot-head") may undermine the observed temperature in the test. The catch pan should be subdivided to reflect the actual area occupied by the sodium, which may affect the comparison between MELCOR and the test.

As noted, the thermal radiation model used in this validation study was the gray gas model. It does not account for the thermal radiation between smoke and heat structures. This may contribute to the observed difference between MELCOR and the test data. It is recommended to implement the enclosure radiation model, which also account for the participating media in the atmosphere (i.e., the gas and smoke).

Finally, the default pool convective heat transfer models do not account for the thermophysical properties of sodium (i.e., assumes water). Because sodium has a much higher thermal conductivity value than water, the use of the heat transfer model must be updated to reflect the high heat transfer rate from liquid sodium to a structure. The validation study showed that the catch pan temperature is much lower than the sodium temperature. To properly address the heat transfer for sodium, the pool heat transfer models should be updated to reflect natural condition from sodium. It is recommended to update the sodium to structure heat transfer rate to match the thermal conditions observed in the test.

Once the above model updates are implemented, it is expected that further improvements of the sodium pool fire model may be identified. The effect of the oxide layers at the pool surface on the oxygen diffusion for the sodium fire is expected to be important. These recommended improvements are expected to improve the MELCOR comparison to F7-1 experiment.

4. SUMMARY AND CONCLUSION

This progress report documents the current work during fiscal year 2019 between Sandia and JAEA on validation of the MELCOR sodium pool fire model. The collaboration enables Sandia and JAEA to improve the sodium fire models in their respective severe accident codes. Descriptions of the current sodium fire model and suggestions for improved physics model are provided in the report.

The sodium fire test F7-1 was calculated by the MELCOR code to investigate capability of the current pool fire model. The MELCOR code predicted the increase of pool and atmosphere temperature due to pool fire. However, the consumption of the pool was higher than measured and the fire extinguished earlier. The pool and atmosphere temperature decreased rapidly after the pool fire ended. This is one of the issues to be examined in future work. The temperature of the heat structures could be improved by using the enclosure radiation heat transfer model and using more accurate view factors. The calculated catch pan temperature was remained low while the measured value is rose to the pool temperature. The low temperature in the MELCOR calculation is attributed to an inappropriate heat transfer coefficient and a lumped response that included regions under the sodium and not under the sodium pool.

Sensitivity calculations were performed to investigate the effects of varying the FHEAT and DAB input parameters. The computational response varying the FHEAT parameter shows a consistent response and its importance in partitioning oxidation energy to the pool versus the atmosphere. The DAB parameter showed almost no difference when it was increased from the default value (i.e., 0 m^2/s) to 5.97×10^{-5} m^2/s. However, when DAB was increased to 1.0×10^{-4} m^2/s, there was a significant increase in the burning rate and the pool and atmosphere temperatures were higher than the base case. Since DAB depends on the instantaneous pressure and temperature, it should be evaluated by using a control function or an internal physics model.

In conclusion, the preliminary validation study on MELCOR's sodium pool fire model has been started. Additional MELCOR input deck refinement may be needed to correctly capture the capability of MELCOR for this F7-1 experiment. Some recommendations have been made for model improvements.

This page left blank

5. REFERENCES

[Clark 2019] Clark, A. J., et al., Modeling and Simulation Activity Sodium Fire Analysis (Task 2-a), SAND2019-3960 PE, U.S.-Japan CNWG Annual Meeting, April 11-12, 2019, Argonne National Laboratory, IL.

[Futagami 1998] Futagami, S., et al., Sodium Pool Combustion Test Run-F7 (Interim Report), PNC TN9410 98-074, Power Reactor and Nuclear Fuel Development Corporation, Oarai, Japan, August 1998.

[Olivier 2010] Olivier, T.J., et al., Metal Fires and Their Implications for Advanced Reactors Part 3: Experimental and Modeling Results, SAND2010-7113, Sandia National Laboratories, Albuquerque, NM October 2010.

[Sandia 2018a] NAC Package Reference Manual in MELCOR Computer Code Manuals, Vol. 2: Reference Manual Version 2.2.11932, SAND2018-13560O, Sandia National Laboratories, Albuquerque, NM, November 2018.

[Sandia 2018b] NAC Package Users Guide in MELCOR Computer Code Manuals, Vol. 1: Users Guide Version 2.2.11932, SAND2018-13559 O, Sandia National Laboratories, Albuquerque, NM, November 2018.

This page left blank

DISTRIBUTION

Email—External (encrypt for OUO)

Name	Company Email Address	Company Name
David Henderson	david.henderson@nuclear.energy.gov	Department of Energy
Damian Peko	damian.peko@nuclear.energy.gov	Department of Energy
Thomas Sowinski	thomas.sowinski@nuclear.energy.gov	Department of Energy
Robert Hill	bobhill@anl.gov	Argonne National Laboratory
Tanju Sofu	tsofu@anl.gov	Argonne National Laboratory
Takashi Takata	takata.takashi@jaea.go.jp	Japan Atomic Energy Agency
Akihiro Uchibori	uchibori.akihiro@jaea.go.jp	Japan Atomic Energy Agency

Email—Internal

Name	Org.	Sandia Email Address
Richard Griffith	8700	rogrif@sandia.gov
Sylvia Saltzstein	8850	sjsaltz@sandia.gov
Mitsuhiro Aoyagi	8852	maoyagi@sandia.gov
Larry Humphries	8852	llhumph@sandia.gov
David Louie	8852	dllouie@sandia.gov
David Luxat	8852	dlluxat@sandia.gov
KC Wagner	8852	kcwagne@sandia.gov
Technical Library	9536	libref@sandia.gov

Sandia National Laboratories

Sandia National Laboratories is a multimission laboratory managed and operated by National Technology & Engineering Solutions of Sandia LLC, a wholly owned subsidiary of Honeywell International Inc. for the U.S. Department of Energy's National Nuclear Security Administration under contract DE-NA0003525.